https://doi.org/10.5194/essd-2026-66
Preprint. Discussion started: 10 February 2026

Open Access Earth System Science Data Discussions

GloWE-8D: a global long-term 8-day wind erosion dataset from 1982 to 2020

Hanbing Zhang[1], Jian Peng[1], Jianquan Dong[2], Zhiwei Yang[1], Yifan Lin[1], Xuebang Liu[1]

[1]College of Urban and Environmental Sciences, Peking University, Beijing 100871, China
[2]School of Landscape Architecture, Beijing Forestry University, Beijing, 100083, China

Correspondence to: Jian Peng (jianpeng@urban.pku.edu.cn)

Abstract. Wind erosion constitutes a critical driver of global land degradation and dust emission, posing persistent threats to ecological security, agricultural production, and human health. Although regional-scale wind erosion assessments exist, there remains a lack of long-term, high spatiotemporal resolution, and publicly available global-scale wind erosion datasets, which has constrained a deeper understanding of its dynamic processes and driving mechanisms. Based on the Revised Wind Erosion Equation (RWEQ), this study constructed a global wind erosion dataset from 1982 to 2020 with an 8-day temporal resolution and a 0.05° spatial resolution. By introducing a residue factor scheme based on growing season identification, the characterization accuracy of wind erosion suppression during vegetation cover periods was enhanced, enabling a more refined depiction of episodic wind erosion features. The dataset revealed that the global annual average wind erosion total from 1982 to 2020 was 539.13 Pg, with severe erosion areas concentrated in the arid and semi-arid regions of the Northern Hemisphere. The wind erosion exhibited a slowly increasing trend, although with significant regional variations. Data validation demonstrated a high spatial consistency between this dataset and the MERRA-2 dust emission data (R^2=0.79), and a significant temporal correlation with coarse-mode aerosol optical depth observations from AERONET stations. Furthermore, comparisons indicated that the results of this study were within the same order of magnitude and showed high correlation with existing regional research. As the first publicly available long-term, high spatiotemporal resolution global wind erosion data product, this dataset provides crucial data support for global and regional dust emission estimation, research on wind erosion process mechanisms, land degradation prevention, and climate change response. The dataset is publicly accessible at https://zenodo.org/records/18245214 (Zhang et al., 2026).

https://doi.org/10.5194/essd-2026-66
Preprint. Discussion started: 10 February 2026

Open Access Earth System Science Data Discussions

1 Introduction

As a key driver of land degradation, wind erosion poses a persistent threat to global ecological security, agricultural production, and human health(Borrelli et al., 2021; Lal, 2003), with its primary and most direct harm being the erosion of land productivity through the removal and transport of nutrient-rich topsoil fine particles, leading to the rapid depletion of soil organic carbon and nutrient pools, thereby directly undermining land productive potential (Alewell et al., 2020; Chappell et al., 2016). This decline in soil quality not only exacerbates food security vulnerability but also is a core mechanism driving land desertification and the degradation of ecosystem services (Chappell et al., 2019; Li et al., 2021). Secondly, the substantial suspended particulate matter generated by wind erosion processes serves as a major source of regional and even global dust events, with these aerosols undergoing long-distance transport and significantly deteriorating air quality in downwind areas, while the pathogens and chemical pollutants they carry pose risks to human respiratory health(Duniway et al., 2019; Ginoux et al., 2004). Furthermore, dust released by wind erosion interacts with the climate system by altering the atmospheric radiation balance and affecting cloud condensation nucleus formation, exerting complex feedbacks on regional and global climate patterns(Zhang et al., 2022b). Consequently, accurate assessment of wind erosion not only forms the scientific basis for understanding global dust source-sink processes and quantifying atmospheric dust loads along with their climatic and environmental effects(Chappell et al., 2023; Tanaka and Chiba, 2006) but is also an indispensable prerequisite for formulating effective land degradation prevention strategies and achieving relevant United Nations Sustainable Development Goals, such as land degradation neutrality, food security, and climate change response(Bexell and Jönsson, 2017; Chappell et al., 2019). Within the context of global climate change, the potential expansion of arid and semi-arid regions and the increased frequency of extreme climate events may further exacerbate wind erosion risks and uncertainties (Borrelli et al., 2023; Huang et al., 2016), making it particularly urgent and critical to systematically clarify the spatiotemporal patterns, dynamic changes, and driving mechanisms of wind erosion on a global scale.

To quantify wind erosion and its impacts, a series of models and methods have been developed in existing research, among which the Revised Wind Erosion Equation (RWEQ) has become one of the most widely used methods for regional-scale wind erosion assessment and spatial mapping due to its good balance between data requirements and simulation accuracy(Funk, 2016). This model has been successfully applied to various typical regions such as Europe, China, Central Asia, and Africa, effectively revealing the spatiotemporal dynamics of local wind erosion and its response to climate change and human activities (Li et al., 2020; Tuo et al., 2018; Wu et al., 2022; Zhao et al., 2021). However, compared to the abundant and in-depth regional studies, overall attention to global-scale wind erosion dynamics remains insufficient (Borrelli et al., 2021; Chu et al., 2024). The current limited global wind erosion assessments have mostly focused on specific years or monthly average estimates (Chu et al., 2024; Sun et al., 2024; Yang et al., 2021), which resulted in a limited ability to capture intra-annual wind erosion dynamics, especially rapid change processes closely related to short-term weather events such as storms and seasonal droughts(Ginoux et al., 2004; Wang et al., 2020). This lack of temporal resolution has constrained a deeper understanding of the instantaneous flux of global dust emission, seasonal transition patterns, and their

https://doi.org/10.5194/essd-2026-66
Preprint. Discussion started: 10 February 2026

coupling mechanisms with atmospheric circulation (Chappell et al., 2023). More importantly, a widely recognized, publicly accessible global wind erosion dataset with long-term temporal coverage and high spatiotemporal consistency has not yet been established (Chu et al., 2024; Sun et al., 2024). Existing studies were either limited by coarse spatial resolution for identifying local source areas or by short time spans for revealing long-term trends, posing challenges for comparative studies on global wind erosion, risk zoning, and the coordinated development of cross-regional environmental policies (Jarrah et al., 2020; Liu et al., 2022b). Therefore, developing a long-term, high-temporal-resolution global wind erosion data product not only fills a current data gap but also provides crucial foundational data support for more finely characterizing the spatiotemporal evolution of dust emission and for validating and improving global climate and dust transport models.

Enhancing the spatiotemporal resolution of wind erosion assessment holds multifaceted scientific value and practical necessity. Firstly, higher spatiotemporal accuracy helps to more accurately reflect the highly heterogeneous and episodic nature of wind erosion processes. The occurrence of wind erosion strongly depends on rapidly changing local conditions such as instantaneous wind speed, surface soil moisture, and vegetation cover (Sharratt et al., 2015; Zhang et al., 2019a). Assessments at monthly or coarser scales often smooth out the fluctuations of these key driving factors, leading to biases in estimating the actual erosion amount, particularly the contribution of extreme events (Chappell et al., 2024; Van Pelt et al., 2004). An 8-day temporal resolution can better align with vegetation growth dynamics and typical weather process cycles, thereby capturing the timing and intensity of wind erosion occurrences at a scale closer to the process level and improving the overall assessment accuracy (Gao et al., 2024; Wei et al., 2023). Secondly, high spatiotemporal resolution assessment results are a prerequisite for achieving refined wind erosion management and targeted policy implementation. They can assist decision-makers in identifying not only regional high-risk areas but also specific hotspot periods and areas within a year, such as during spring high-wind periods (Lackóová et al., 2023; Zhang et al., 2021). This can guide the implementation of targeted measures like seasonal cover crop planting and emergency sand barrier deployment, optimizing the layout and management efficiency of ecological projects (Chi et al., 2019; Zhou et al., 2025). However, constructing a high-resolution global wind erosion dataset faces significant challenges, with the core issues lying in the global consistency, spatiotemporal continuity, and reliability of the driving data (Jarrah et al., 2020). The acquisition and processing of key parameters such as near-surface wind speed, vegetation coverage, and soil moisture are particularly crucial (Ma et al., 2025). Existing research has addressed these challenges by developing corresponding data assimilation and scale conversion methods through the integration of multi-source remote sensing products, reanalysis meteorological data, and ground observations (Chappell et al., 2023; Wang et al., 2020). These efforts have laid the foundation for developing more reliable high-resolution global wind erosion models and also highlight the feasibility and significant value of producing a global wind erosion dataset with both high spatiotemporal resolution and a long temporal span under current data and technological conditions.

Building upon an in-depth analysis of the current status of global wind erosion assessment and the urgent need for high-resolution data, this study constructed, for the first time, a global wind erosion assessment dataset spanning 1982–2020 with an 8-day temporal resolution and a 0.05° spatial resolution. This dataset was developed based on the RWEQ, integrating multi-source data, including reanalysis meteorological data, vegetation cover products, land use, and soil properties datasets.

https://doi.org/10.5194/essd-2026-66
Preprint. Discussion started: 10 February 2026

By introducing a residue factor scheme based on growing season identification, the assessment accuracy of wind erosion suppression during vegetation cover periods was enhanced. This study not only achieved continuous, high spatiotemporal resolution monitoring of global wind erosion processes but also systematically revealed the spatiotemporal patterns, change trends, and seasonal characteristics of wind erosion over the past four decades, providing the first long-term, high spatiotemporal resolution open-access data product for global wind erosion research.

2 Materials and Methods

2.1 Data Sources and Processing Procedures

This study primarily assessed wind erosion based on the RWEQ and validated the results using aerosol observations and simulated dust emission data (Figure 1). Meteorological data, including temperature, precipitation, wind speed, snow depth, and evapotranspiration, were obtained from the ERA5 reanalysis dataset provided by the European Centre for Medium-Range Weather Forecasts (ECMWF), which is based on ECMWF's fifth-generation atmospheric reanalysis of the global climate (https://cds.climate.copernicus.eu/datasets). Key variables selected included 10m wind speed, 2m temperature, precipitation flux, snow depth flux, and solar radiation flux, with a daily temporal resolution and a 0.1° spatial resolution. These data were resampled to 0.05° without altering their values. Fractional vegetation cover (FVC) data were obtained from the GLASS FVC product, with an 8-day interval (46 periods per year) and a 0.05° spatial resolution (https://www.glass.hku.hk/download.html). Land use data were sourced from the GLC_FCS30D product (global 30 m land-cover dynamic monitoring product with a fine classification system) with a 30m spatial resolution (https://data.casearth.cn/thematic/glc_fcs30/314) (Zhang et al., 2024c). For years before 2000, when data were unavailable at annual intervals, the temporally closest available data were used. As the final wind erosion assessment resolution was 0.05°, the area proportion of different land use types within each 0.05° grid cell was calculated. Wind erosion was then assessed according to algorithms specific to each land use type, and the final wind erosion result for the 0.05° pixel was obtained by weighting these assessments based on the area proportions. Digital Elevation Model (DEM) data were sourced from the Copernicus DEM provided by ESA, with a 30m resolution (https://dataspace.copernicus.eu/explore-data/data-collections/copernicus-contributing-missions/collections-description/COP-DEM). For soil data, the primary properties used were sand, clay, and silt content, organic matter content, and calcium carbonate content. The sand, clay, silt, and soil organic matter content were obtained from SoilGrids, which provides numerical soil property estimates for seven standard depths (0, 5, 15, 30, 60, 100, and 200 cm) (https://isric.org/explore/soilgrids). Based on model requirements, data from the top four depths were weighted and averaged to derive surface soil data required by the RWEQ model. The spatial resolution was 250m. Calcium carbonate content was derived from the Harmonized World Soil Database (HWSD), using the surface calcium carbonate content field (T_CACO3: Real), with a 1km resolution (https://www.fao.org/soils-portal/data-hub/soil-maps-and-databases/harmonized-world-soil-database-v20). All datasets were finally resampled to a 0.05° spatial resolution before being input into the RWEQ. For validation, dust emission data were obtained from the monthly-scale MERRA2

https://doi.org/10.5194/essd-2026-66
Preprint. Discussion started: 10 February 2026

tavgU_2d_adg_Nx dataset (https://disc.gsfc.nasa.gov/datasets). Aerosol observation data were sourced from the Aerosol Optical Depth (V3)-Solar dataset (SDA2.0 product) of the AERONET site data. The Coarse_Mode_AOD_500nm was selected to represent observed dust concentration (https://aeronet.gsfc.nasa.gov/new_web/download_all_v3_aod.html).

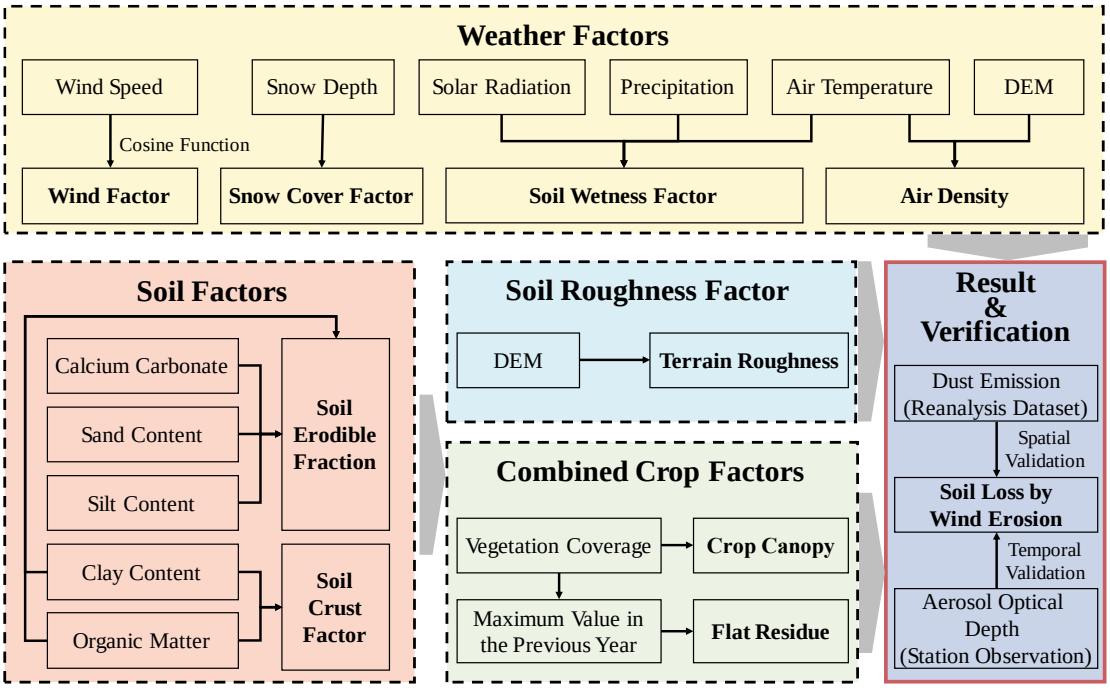

Figure 1. Production and verification process for the global wind erosion dataset

2.2 Wind Erosion Assessment Method

The RWEQ is designed to estimate regional soil wind erosion with a high spatial and temporal resolution over an extended time series and effectively evaluate wind erosion (Fryrear et al., 2000). This model is an experience-based process model that can estimate soil erosion and transportation at the soil surface and at up to 2 m above the surface. It is also widely used to estimate soil loss on a regional scale and can provide a basis for the prevention and control of land desertification.

$$Q_{max} = 109.8(WF \cdot EF \cdot SCF \cdot K' \cdot COG) \quad (1)$$

$$S = 150.71(WF \cdot EF \cdot SCF \cdot K' \cdot COG)^{-0.3711} \quad (2)$$

$$S_L = \frac{2x}{S^2} Q_{max} \left(\frac{x}{S}\right)^2 \quad (3)$$

where Q_{max} (kg/m) is the maximum transport capacity and S (m) is the critical field length, which is defined as the distance at which 63.2% of the maximum transport capacity is reached. Q_{max} and S are derived from the weather factor (WF) in kg/m; the dimensionless factors are the soil erodibility factor (EF), the soil crust factor (SCF), the soil roughness factor (K′), and the combined vegetation factor (COG); SL (kg/m^2) is the rate of soil loss caused by wind erosion, which is also referred to as the wind erosion modulus; and x is the distance from the upwind edge of the field in m.

https://doi.org/10.5194/essd-2026-66
Preprint. Discussion started: 10 February 2026

2.2.1 Weather Factors

$$WF = \frac{wf \cdot \rho}{N \cdot g} \cdot SW \cdot SD \tag{4}$$

$$wf = \sum_{i=1}^{N} U_2 \cdot (U_2 - U_t)^2 \tag{5}$$

where wf is wind factor (m^3/s^3);ρ is air density (kg/m^3); g is acceleration due to gravity (m/s^2); SW is soil wetness; SD is the snow cover factor; U_2 (m/s) is wind speed at the height of 2 m; U_t (m/s) is the threshold wind speed at 2 m (assumed wind speed of 5 m/s); N_d is the number of days in the period; N is the number of wind speed observations.

We need to convert wind speeds at 10 meters to wind speeds at 2 meters using the following formula.

$$U_2 = U_z \cdot \frac{4.87}{ln(6.78 \cdot z - 5.42)} \tag{6}$$

Where U_2 (m/s) represents the wind speed at a height of 2 meters, and U_z (m/s) denotes the wind speed value at a given height z (in meters); z = 10 in this study.

Considering the impact of temporal and measuring resolutions of wind erosion data on assessment accuracy, we resampled daily wind speeds using a cosine function. The specific calculation method is as follows (Guo et al., 2012, p.201):

$$W_n = W_{ave} \cdot \left(1 + COS\left(\frac{n \cdot \pi}{12}\right)\right) \tag{6}$$

where W_n is the simulated wind speed (m/s), W_{ave} is the daily average wind speed (m/s), and n=24.

$$\rho = 348\left(\frac{1.013 - 0.1183EL + 0.0048EL^2}{T}\right) \tag{7}$$

ρ is calculated from the elevation EL (km) and the absolute temperature T (Kelvins).

$$SW = \frac{ET_P - (R + I)\frac{R_d}{N_d}}{ET_P} \tag{8}$$

$$ET_P = 0.0162\left(\frac{SR}{58.5}\right) \cdot (DT + 17.8) \tag{9}$$

$$SD = 1 - P(Snowdeep > 25.4mm) \tag{10}$$

where ET_P is the potential relative evapotranspiration (mm); $R + I$ (mm) is precipitation and irrigation; R_d is the number of precipitation and irrigation days; SR (cal/cm^2) is solar radiation; DT (°C) is average temperature; P is probability of snow depth >25.4 mm.

2.2.2 Soil Factors

The soil erodibility factor (EF) and the soil crust factor (SCF) were calculated as:

$$EF = \frac{29.09 + 0.31Sa + 0.17Si + 0.33\frac{Sa}{Cl} - 2.59OM - 0.95CaCO_3}{100} \tag{11}$$

https://doi.org/10.5194/essd-2026-66
Preprint. Discussion started: 10 February 2026

$$SCF = \frac{1}{1 - 0.0066Cl^2 + 0.021OM^2} \quad (12)$$

where *Sa* (%) is the sand content; *Si* (%) is the silt content; *Sa/Cl* is sand to clay ratio; *OM* (%) is the organic matter content; *CaCO3* (%) is the calcium carbonate content.

2.2.3 Soil Roughness Factors

The soil roughness factor (*K′*) is related to the chain random roughness *Crr* (cm), and soil ridge roughness *Kr* (cm), and it was calculated as:

$$K' = e^{(1.86Kr - 2.41Kr^{0.934} - 0.127Crr)} \quad (13)$$

In this study, terrain roughness was used as a substitute for soil roughness as equation 14. *Crr* is considered as 0 in this study due to the difficulty in data collection.

$$Kr = 0.2\frac{\Delta H^2}{L} \quad (14)$$

where *Kr* (cm) is the terrain roughness coefficient, *ΔH* (cm) is the average elevation difference between peaks and valleys in the area, and *L* (cm) is the average distance between adjacent peaks (separated by valleys) or between consecutive ridges. To ensure the accuracy of roughness coefficient calculations, we employ DEM data with 30m resolution for computation, subsequently resampled to 0.01°.

2.2.4 Combined Crop Factors

The COG consists of the soil loss ratio coefficients for growing crop canopy (SLR_c), the soil loss ratio coefficients for flat cover (SLR_f), and the soil loss ratio coefficients for plant silhouettes (SLR_s). SLRs is only applicable for estimating wind erosion in cultivated areas. For reasons analogous to those for lodged crop residues, they are excluded from this study to reduce uncertainties in wind erosion assessment.

$$COG = SLR_c \cdot SLR_f \cdot SLR_s \quad (15)$$

$$SLR_c = e^{-5.614cc^{0.7366}} \quad (16)$$

$$SLR_f = e^{-0.0438SC} \quad (17)$$

Where *cc* is the vegetation cover, *SC* is the surface coverage of dead vegetation. This study implemented differentiated settings for flat residues across different land use types: forest was not applicable for this parameter. The residue amount for cropland was set to zero due to the lack of data on crop types and farming practices, and the complexity and higher uncertainty associated with modeling decomposition processes. While this setting might slightly overestimate wind erosion, it avoids introducing greater errors. For grassland, the residue amount was calculated using an empirical formula based on the vegetation cover from the previous growing season (Gong et al., 2014). Furthermore, flat residues were only applied

https://doi.org/10.5194/essd-2026-66
Preprint. Discussion started: 10 February 2026

during the non-growing season. The start and end dates of the growing season were determined based on the 50% threshold (Gu et al., 2022) method established in existing research (Shi et al., 2025).

2.3 Data Evaluation and Analysis

The temporal trend of wind erosion at each grid was quantified using Theil-Sen slope estimation, while trend significance was evaluated through the Mann-Kendall test. This dual-filtering approach ensured that modeled relationships could reflect ecologically meaningful changes in green landscape ecological quality rather than random fluctuations. This study first employed Sen's slope estimator to calculate the slope β of the wind erosion time series. When $\beta > 0$, the overall trend was upward; when $\beta < 0$, the trend was downward; and when $\beta = 0$, no significant trend was observed. Sen's slope estimator constituted a non-parametric computational method that could demonstrate robust resistance to outliers. The median function was applied to compute Sen's estimator for the time series as follows:

$$\beta = Median\left(\frac{x_j - x_i}{j - i}\right), \forall j > i \tag{18}$$

The Mann-Kendall test was a non-parametric statistical method employed to determine the significance of temporal trends in sequential data. The test statistic S represented the sum of step function values derived from pairwise differences between all distinct samples in the target sequence. Significance assessment utilized the Z-score, where $|Z| \geq 1.96$ (indicating significance at the 95% confidence level, with $Z > 0$ for an increasing trend, and $Z < 0$ for a decreasing trend) denoted a statistically significant trend.

$$S = \sum_{i=1}^{n-1} \sum_{j=i+1}^{n} \mathrm{sgn}\left(x_j - x_i\right) \tag{19}$$

$$Z = \begin{cases} \dfrac{s-1}{\sqrt{Var(S)}} & S > 0 \\ 0 & S = 0 \\ \dfrac{s+1}{\sqrt{Var(S)}} & S < 0 \end{cases} \tag{20}$$

The variance *Var(S)* was computed as:

$$Var(S) = \frac{n(n-1)(2n+5)}{18} \tag{21}$$

In this study, concentration and interannual variability were employed to characterize the seasonal features of wind erosion. The peak period was first defined as a local maximum, meaning its wind erosion value was greater than those of the five preceding and five subsequent periods and also exceeded the annual mean value. The Wind Erosion Concentration Period (WECP) was defined as the peak period plus these five preceding and five subsequent periods. Furthermore, two identified WECP were not allowed to overlap; in case of overlap, only the period with the higher peak wind erosion intensity

https://doi.org/10.5194/essd-2026-66
Preprint. Discussion started: 10 February 2026

Open Access Earth System Science Data Discussions

was retained. The concentration was calculated as the ratio of the cumulative wind erosion during the WECP to the total annual wind erosion, using the following formula:

$$Concentration = \frac{\sum_{t-5}^{t+5} SL_i}{SL_{year}} \quad (22)$$

Where SL_i is the wind erosion in the i-th period, t is the peak period, and SL_{year} is the annual total wind erosion.

Volatility is defined as the degree of fluctuation in wind erosion during a specific period within a year. Lower volatility indicates greater stability. The primary calculation method is as follows:

$$Volatility_i = \frac{\mu_i}{\sigma_i} \quad (23)$$

where μ_i and σ_i are the mean and variance of wind erosion for the i-th period during the 1982–2020, respectively.

3 Result

3.1 Global Wind Erosion Patterns

The global annual average total wind erosion was 539.13 Pg. It exhibited a spatially heterogeneous distribution characterized by high values in arid regions and low values in humid regions, with concentrations in middle and low latitudes and scattered distribution in high latitudes (Figure 2a). High wind erosion values were primarily concentrated in the arid and semi-arid areas of the middle and low latitudes in the Northern Hemisphere, including the Sahara Desert and its surrounding areas, the entire Arabian Peninsula, and parts of the arid regions in Central Asia. In the Southern Hemisphere, high wind erosion areas were scattered across the arid regions of southern Africa, the central-western deserts of Australia, and some arid areas in South America. In contrast, wind erosion intensity was generally low in humid regions near the equatorial low latitudes and in the subarctic and Arctic high-latitude regions, with most areas experiencing an intensity below 0.50 kg/m²/year. Wind erosion intensity was particularly weak across most of North America, the entirety of Europe, and parts of the humid regions in East Asia.

At the national scale (Figure 2b), the distribution of total wind erosion was highly concentrated in countries within arid regions of Africa and the Middle East. Algeria ranked first globally with a total wind erosion of 69.78 Pg, followed by Libya (50.75 Pg) and Sudan (50.56 Pg). The combined total wind erosion of the top ten countries accounted for 68.88% of the global total. In contrast, the total wind erosion for most countries in Europe and the Americas was extremely low: Russia was only 0.25 Pg, Canada 0.27 Pg, the United States 2.25 Pg, and Brazil 0.13 Pg. The annual average wind erosion for most European countries was even less than 0.01 Pg, all far below the global average.

Countries with high wind erosion intensity did not completely overlap with the top ten countries in terms of total wind erosion (Figure 2b). Western Sahara, with a wind erosion intensity of 88.91 kg/m², was the region with the highest wind erosion intensity globally, although its total wind erosion only ranked ninth. Some countries not in the top ten for total wind erosion were among the world's leaders in wind erosion intensity. For instance, Kuwait had a total wind erosion of only 0.70

https://doi.org/10.5194/essd-2026-66
Preprint. Discussion started: 10 February 2026

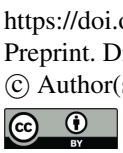

Open Access Earth System Science Data Discussions

Pg but an intensity as high as 40.00 kg/m², ranking second globally. Qatar, with a total of merely 0.38 Pg, had an intensity of 32.72 kg/m², placing it within the top five for intensity. Furthermore, countries like Bahrain (total 0.01 Pg, intensity 16.56 kg/m²), Aruba (total 0.003 Pg, intensity 18.22 kg/m²), Sint Maarten (total 0.0004 Pg, intensity 7.93 kg/m²), and Montserrat (total 0.0003 Pg, intensity 2.65 kg/m²)—mostly small territories with extreme aridity—exhibited a striking contrast between their prominent wind erosion intensity and their low levels of total wind erosion. Overall, the national distribution of wind erosion intensity was closely related to climatic aridity and surface vegetation cover, with countries characterized by dry conditions, low precipitation, and sparse vegetation generally experiencing higher wind erosion intensity.

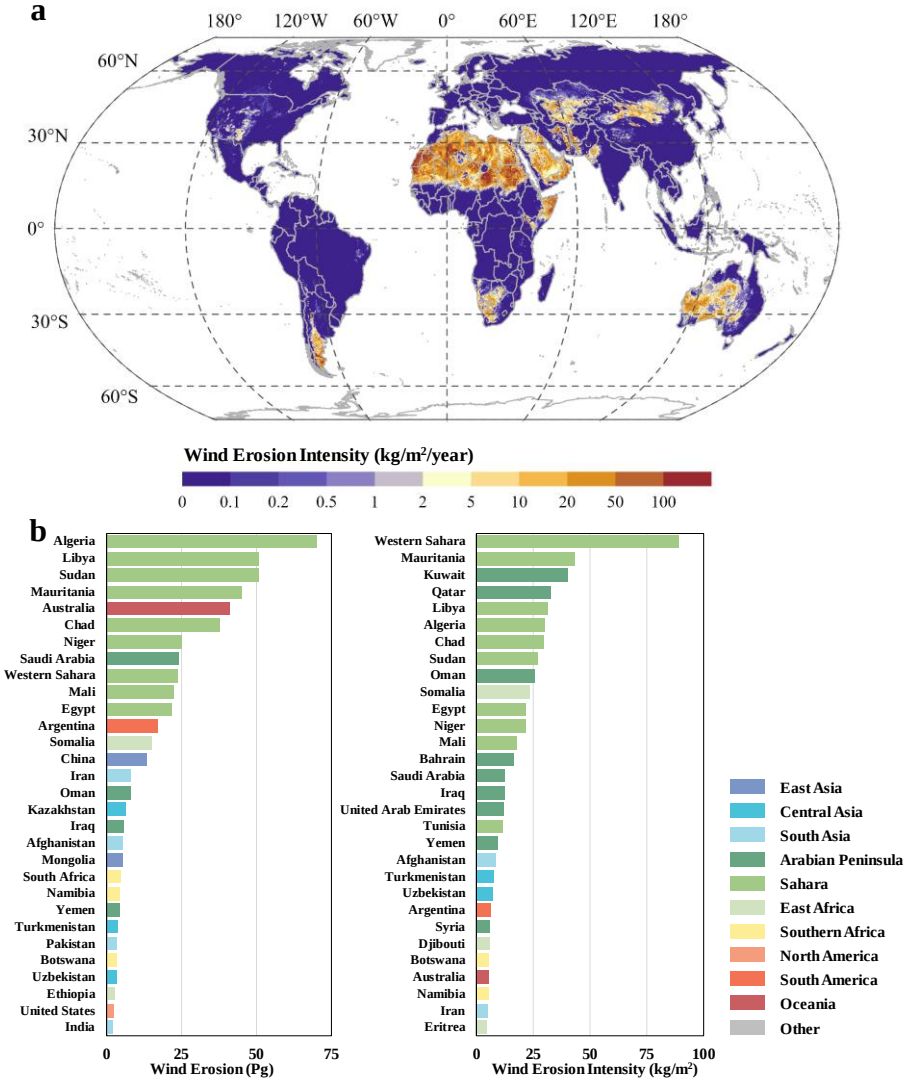

Figure 2 Global wind erosion from 1982 to 2020 (a, spatial distribution of wind erosion; b, national rankings of total wind erosion and wind erosion intensity)

https://doi.org/10.5194/essd-2026-66
Preprint. Discussion started: 10 February 2026

Open Access Earth System Science Data Discussions

3.2 Global Wind Erosion Trends

Global wind erosion exhibited a slowly increasing trend from 1982 to 2020, with distinct spatial heterogeneity and temporal dynamic characteristics across different regions (Figure 3). The global annual average total wind erosion increased from 520.16 Pg during 1982-1990 to 527.18 Pg during 1991-2000, further rising to 550.64 Pg in 2001-2010, and reaching 556.63 Pg in 2011-2020, representing an approximate increase of 2.33% per decade across these four decades.

The Sahara (annual average total wind erosion 350.35 Pg), the Arabian Peninsula (44.92 Pg), East Africa (19.50 Pg), and North America (2.74 Pg) exhibited steady increases in wind erosion, with growth rates of 2.96% per decade, 3.31% per decade, 3.66% per decade, and 6.78% per decade, respectively. South Asia (annual average total wind erosion 18.65 Pg) was the only region where wind erosion decreased every decade, with a cumulative decline of 6.56%. Central Asia (12.75 Pg), Southern Africa (12.04 Pg), and South America (17.01 Pg) were characterized as stable fluctuation areas with low to moderate intensity. East Asia (18.39 Pg) showed a unique trend of initially increasing and then decreasing, with the total wind erosion from 2011-2020 declining by 14.12% compared to the previous decade. Australia (41.07 Pg), in contrast, experienced an initial decrease of 10.51%, followed by fluctuations of less than 0.5% per decade in later periods, indicating an overall trend towards stabilization.

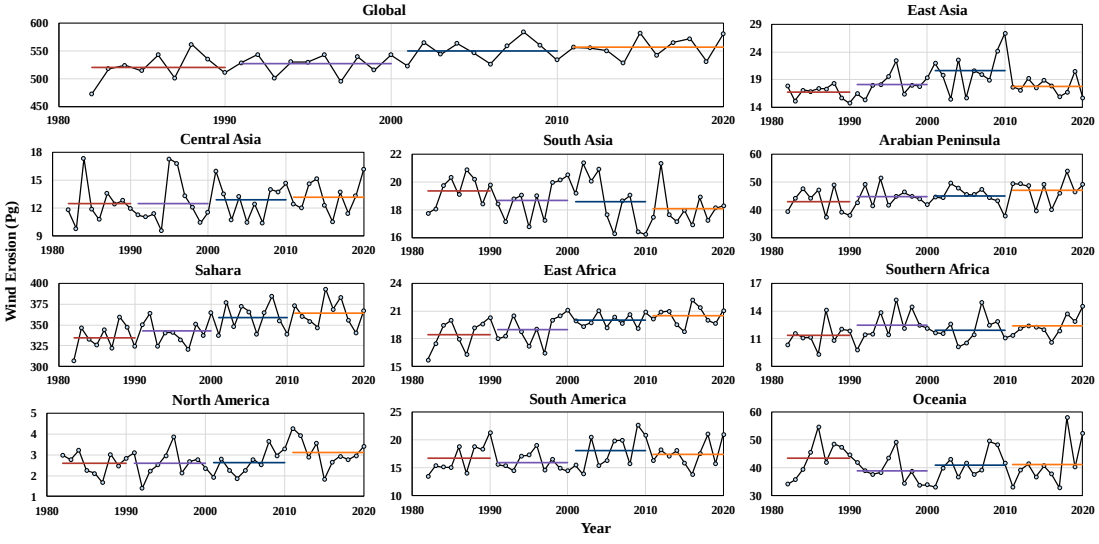

Figure 3. Interannual variations in wind erosion across representative regions

Results from the pixel-based trend analysis (Figure 4a) indicated that areas with significantly increasing wind erosion were primarily concentrated in the arid and semi-arid areas spanning from low to middle latitudes in the Northern Hemisphere. The core distribution areas encompassed the entirety of the Sahara Desert in northern Africa and its surrounding peripheral regions, the northeastern part of the East African Plateau, and the entire Arabian Peninsula. Additionally, these areas included central Kazakhstan and southern Mongolia in Central Asia, northern Argentina in southeastern South America, and parts of the arid regions in southern Africa. Conversely, areas exhibiting a significant

https://doi.org/10.5194/essd-2026-66
Preprint. Discussion started: 10 February 2026

decrease in wind erosion were mainly distributed across the South Asian subcontinent, central-western Australia in Oceania, southern Afghanistan, western Iraq, and northern Oman in the Middle East, southwestern Russia in Eastern Europe, Turkmenistan in Central Asia, and western Senegal in West Africa, among other regions.

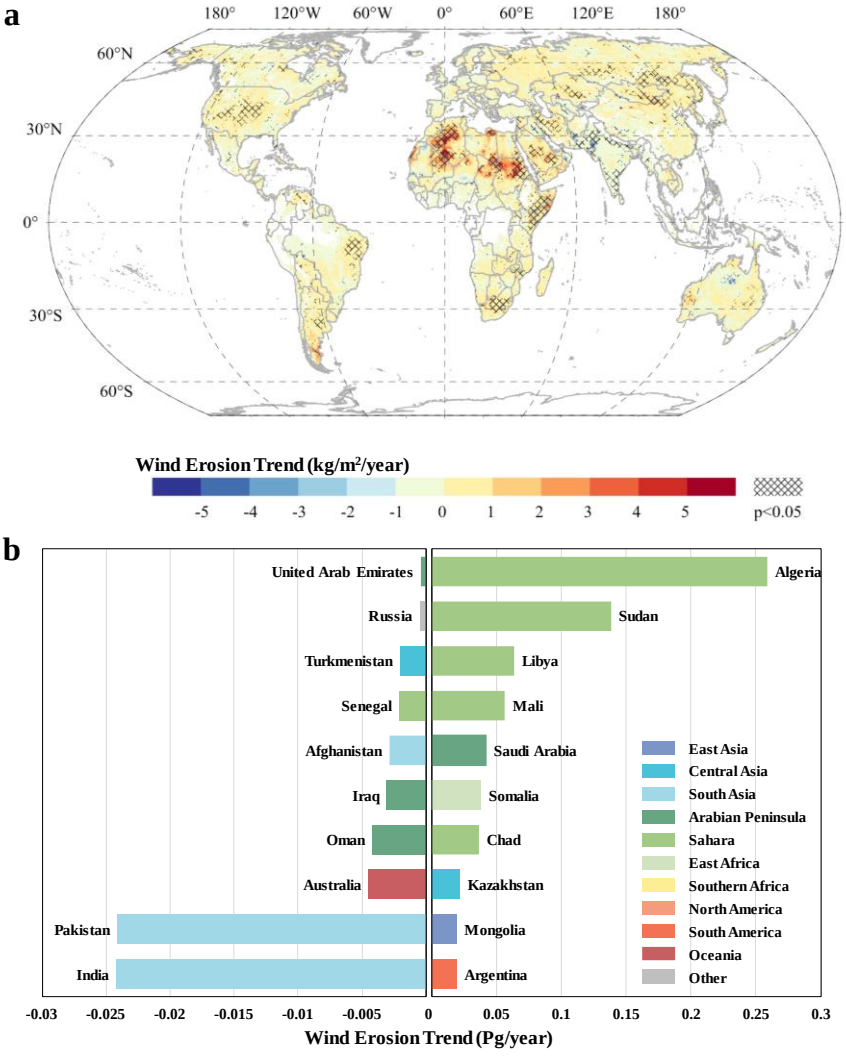

Figure 4. Global wind erosion trends from 1982 to 2020 (a, spatial distribution of wind erosion trends and significant; b, national ranking of total wind erosion changes)

Furthermore, we quantified the national-scale ranking of the total wind erosion change considering only statistically significant areas (Figure 4b). Among countries with significantly increasing wind erosion, Algeria ranked first with a total wind erosion change of 0.26 Pg/year, making it the country contributing most to the global increase in wind erosion, followed by Sudan (0.14 Pg/year), Libya (0.06 Pg/year), Mali (0.06 Pg/year), Saudi Arabia (0.04 Pg/year), and Somalia (0.04 Pg/year). These countries are all concentrated in the Sahara Desert and surrounding regions of North and East Africa,

https://doi.org/10.5194/essd-2026-66
Preprint. Discussion started: 10 February 2026

with Algeria and Sudan showing far greater increases in wind erosion than other countries, together accounting for nearly 60% of the total increase from globally significant areas. Among countries with significantly decreasing wind erosion, India and Pakistan tied for first place with an identical rate of -0.024Pg/year, making them the two countries with the most pronounced global decrease in wind erosion. The decreases in other countries were generally smaller than the magnitude of increase in the countries with rising trends. Overall, countries with significantly increasing wind erosion were primarily concentrated in the core arid areas of northern and eastern Africa, while countries with significantly decreasing wind erosion were mostly distributed in the semi-arid transition areas of South Asia, Oceania, and the Middle East.

3.3 Seasonal Characteristics of Wind Erosion

Regarding seasonal distribution (Figure 5a), most arid regions exhibited a unimodal distribution pattern except for the Arabian Peninsula. The peak wind erosion periods in the Northern Hemisphere regions all occurred in the first half of the year, while those in the Southern Hemisphere occurred in the second half. East Africa had the highest concentration (peak period 25, wind erosion 1.36 Pg, concentration 66.51%), followed by South Asia (peak period 24, wind erosion 1.07 Pg, concentration 52.28%) and East Asia (peak period 15, wind erosion 1.08 Pg, concentration 47.44%); concentrations in other regions were all below 40% (Figure 5b). The Sahara, as the core area with the highest global wind erosion intensity, reached its maximum wind erosion value in period 11 (11.37 Pg). The cumulative wind erosion during this peak period and its surrounding intervals totaled 115.33 Pg, yet this accounted for only 32.92% of its annual total, indicating it experiences intense wind erosion throughout the year. The Arabian Peninsula, as the only region with a bimodal distribution, exhibited two peaks in period 11 (wind erosion 1.96 Pg, concentration 35.35%) and period 25 (wind erosion 2.02 Pg, concentration 36.73%). North America had the lowest concentration (peak period 13, wind erosion 0.14 Pg, concentration 23.88%).

The results of the variability analysis (Figure 5c) indicated that Central Asia exhibited the highest annual mean wind erosion variability (0.93), followed by North America (0.79) and East Asia (0.75). In contrast, the Sahara region, despite having the highest annual mean wind erosion, showed the lowest annual mean variability (0.33), which was only 35.27% of that in Central Asia. The variability during the wind erosion concentration period was significantly lower than the annual mean across all regions, indicating more stable wind erosion conditions during these peak periods. Notably, in East Africa (concentration period variability 0.15) and South Asia (concentration period variability 0.27), the variability during the concentration period decreased by 0.29 and 0.36, respectively, compared to their annual means. The differences between the concentration period and annual mean variability were relatively small in Southern Africa, the Sahara, and North America, at only 0.4, 0.5, and 0.5, respectively. In other regions, the decrease in variability during the concentration period compared to the annual mean ranged between 0.1 and 0.2.

https://doi.org/10.5194/essd-2026-66
Preprint. Discussion started: 10 February 2026

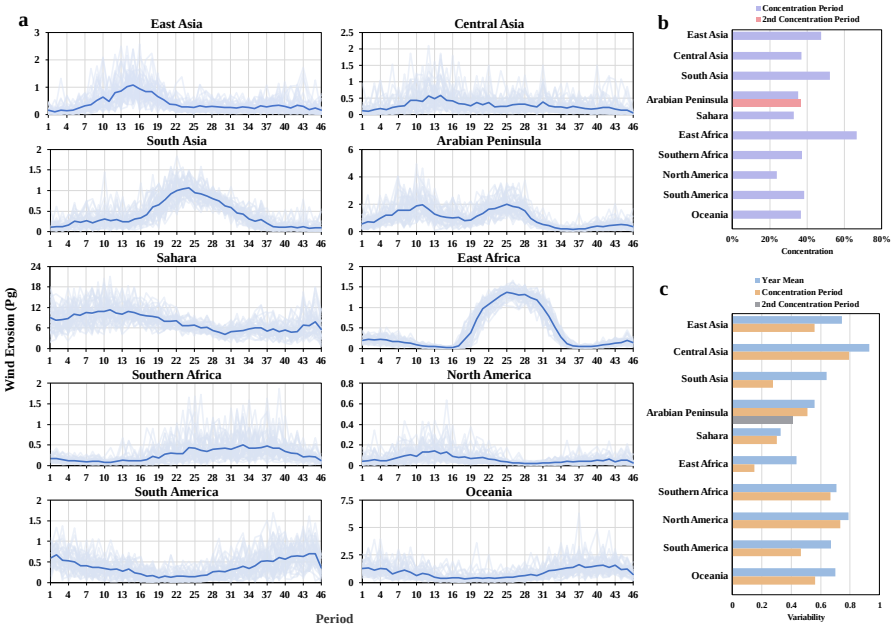

325

Figure 5 Seasonal wind erosion characteristics in different arid regions (a, seasonal distribution of wind erosion; b, concentration; c, fluctuation in each region)

3.4 Dataset Evaluation and Validation

To validate the assessment results of this study on a spatial scale, we further compared them with annual average dust emission data for the same period (Figure 6a). To mitigate potential influences from outliers, the wind erosion intensity data were grouped into intervals of 1 kg/m²/year, and the mean value of each group was used as a representative sample to analyze its relationship with the corresponding mean dust emission. As shown in Figure 6b, a significant cubic relationship was observed between them (R^2=0.79, p<0.001), indicating that the spatial distribution of the wind erosion assessment results in this study is highly consistent with existing simulated dust emission data.

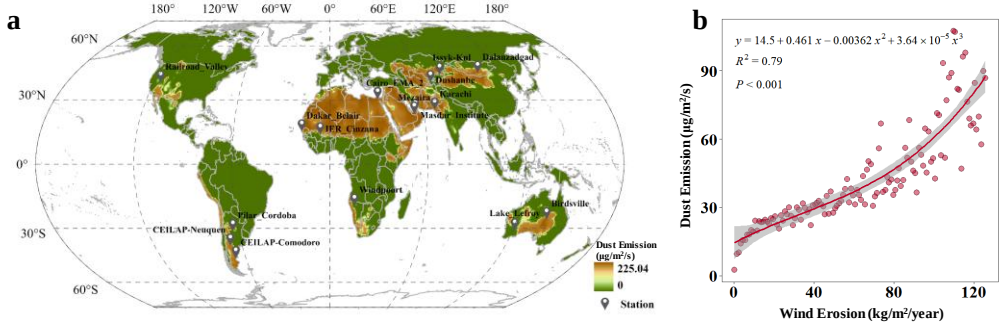

335

Figure 6 Comparison of dust-emission data with wind erosion assessment results (a, Spatial distribution of dust emissions from 1982 to 2020; b, fitting of dust emissions and wind erosion)

https://doi.org/10.5194/essd-2026-66
Preprint. Discussion started: 10 February 2026

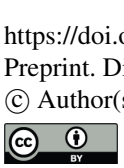

Open Access Earth System Science Data Discussions

Concurrently, to verify the reliability of the wind erosion assessment results from this study on a temporal scale, a comparative analysis was conducted with site-observed coarse-mode aerosol optical depth. Given the 8-day temporal resolution of the wind erosion data in this study, which does not align with monthly-scale dust emission data, daily coarse-mode aerosol optical depth observations from 16 stations located in typical wind erosion regions were selected (Figure 6a). Considering the spatial dispersion and temporal lag during dust transport, for each station, the cumulative total wind erosion within a 1000 km radius surrounding it for the current and preceding periods was calculated and then correlated with the station's daily coarse-mode aerosol optical depth. The results showed that a significant positive correlation was observed at the vast majority of stations (Figure 7). Although the R^2 was relatively low for a few individual stations—potentially due to the influence of local wind direction, wind speed, and atmospheric processes on dust transport, leading to some discrepancy between the fixed spatiotemporal cumulative wind erosion and the station-measured optical depth—the overall temporal variation of total wind erosion exhibited a consistent and significant positive correlation with coarse-mode aerosol optical depth. This result supports the accuracy of the temporal trends in the wind erosion assessment conducted in this study.

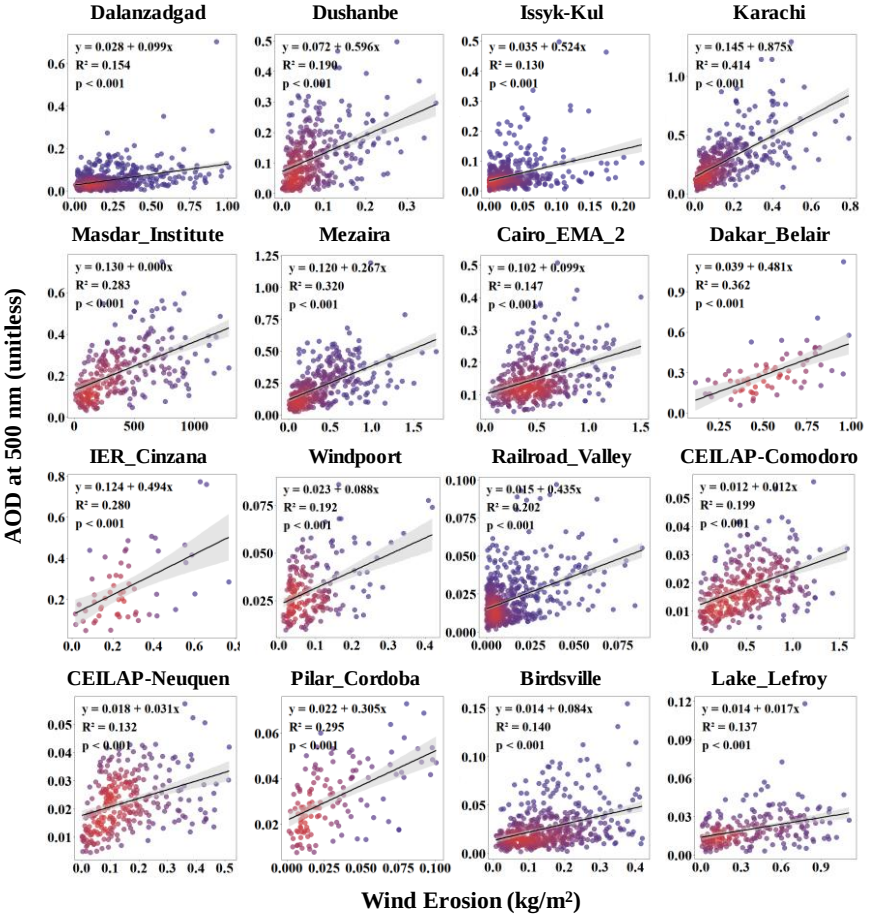

Figure 7. Temporal comparison of gross optical depth at stations with wind erosion assessment results from this study

https://doi.org/10.5194/essd-2026-66
Preprint. Discussion started: 10 February 2026

Open Access Earth System Science Data Discussions

4 Discussion

4.1 Comparison with Existing Wind Erosion Assessment Results

This study, based on the RWEQ model and utilizing high spatiotemporal resolution input data (0.05°, 8-day), innovatively introduced a dynamic residue factor scheme tied to the growing season to produce a global wind erosion dataset spanning 1982–2020. Compared with other recent global studies also based on RWEQ, the assessment results from this study were slightly higher in total amount than some(Chu et al., 2024; Sun et al., 2024) and slightly lower in per-unit-area intensity than studies that did not consider the residue factor (Yang et al., 2021), yet all results remained within the same order of magnitude. These discrepancies likely stem primarily from differences in spatial resolution, temporal step length, and the more refined characterization of the residue factor. Higher resolution allows the model to capture more localized wind erosion hotspots and transient erosion events, potentially leading to a higher global total estimate; conversely, the reasonable exclusion of the residue factor during the growing season effectively avoids overestimating the wind erosion protection provided by vegetation cover, resulting in more reasonable wind erosion estimates. Therefore, the results of this study offer advantages in terms of the physical realism of process representation and the richness of spatial detail, providing a more reliable data foundation for further understanding the spatiotemporal dynamics of global wind erosion.

Furthermore, we collected regional-scale wind erosion assessments from existing studies (Table 1). A comparative analysis revealed a strong agreement between the results of this study and the existing literature. The findings were all within the same order of magnitude, and the Pearson correlation coefficient for wind erosion intensity between them reached 0.86. Minor discrepancies could be attributed to objective differences in research methodology, data sources, and procedural details. Specifically, for several typical regions in China, such as Inner Mongolia, the Hexi Corridor, and the Loess Plateau, the assessment results from this study aligned well with or fell within a reasonable range of concurrent research. On a larger scale, estimates for Central Asia and Southern Africa also closely approximated those of prior studies. Although a certain degree of overestimation was observed in some localized areas, such as the Mu Us Sandy Land—potentially due to differences in data sources and parameterization—the overall trends were consistent, and all results remained within the same order of magnitude. In summary, this global assessment not only demonstrates strong agreement with existing studies in most regions but also reduces comparability biases between regional results through a consistent methodology and data sources, providing a credible data foundation for understanding long-term wind erosion dynamics and their driving mechanisms.

Table 1. Comparison of regional-scale wind erosion assessments in existing studies with the results of this study

Study Period	Method	Study Area	Wind Erosion Intensity (kg/m2/year)	Wind Erosion Intensity in This Study(kg/m2/year)	Reference
1990-2015	RWEQ	China	1.25	1.44	(Chi et al., 2019)
2000-2020	RWEQ	Drylands in China	3.85	2.29	(Feng et al., 2025)

https://doi.org/10.5194/essd-2026-66
Preprint. Discussion started: 10 February 2026

2000-2012	RWEQ	Agricultural Pastoral Ecotone in northern China	1.57-2.73	1.77	(Zhang et al., 2022a)
2000-2012	RWEQ	Agricultural Pastoral Ecotone in northern China	2.59	1.77	(Liu et al., 2022a)
	WEPS		5.26		
	IWEMS		5.87		
	NWESMC		1.26		
2000-2020	RWEQ	Northeast, China	0.15	0.49	(Wang et al., 2022)
1986-2005	Quantitative retrieval model	Mu Us Sandy Land, China	1.57-1.69	3.52	(Yue et al., 2015)
2000-2020	RWEQ	Mu Us Sandy Land, China	0-1.36	4.13	(Liu et al., 2023)
1990-2020	RWEQ	Kubuqi Desert, China	4.54	6.78	(Dang et al., 2022)
1982-2015	RWEQ	Hexi Region,China	6.77	6.63	(Lin et al., 2021)
2000-2018	RWEQ	Northern Slope of the Tianshan Mountains, China	6.56	3.01	(Wang et al., 2024)
2000-2021	RWEQ	Loess Plateau, China	0.40	1.00	(Tao et al., 2024)
1990-2018	RWEQ	Yellow River Basin, China	0.57-0.84	0.87	(Chi et al., 2022)
2001-2016	RWEQ	Horqin Sandy Land, China	0.55	1.77	(Zhang et al., 2021)
2001-2010	RWEQ	Inner Mongolia, China	3.40-4.82	5.39	(Jiang et al., 2016)
1990-2015	RWEQ	Inner Mongolia, China	3.56	4.70	(Zhang et al., 2018)
2000-2021	RWEQ	Inner Mongolia, China	2.86	4.85	(Zhang et al., 2024b)
1990-2022	RWEQ	Inner Mongolia, China	3.57	4.61	(Mei et al., 2025)
1982-2018	RWEQ	Mongolia plateau	4.65	3.84	(Wei et al., 2023)
2010	WEQ	Mongolia	0.27-2.75	4.82	(Mandakh et al., 2016)
1986-2005	RWEQ	Central Asia	1.60	3.10	(Li et al., 2020)
2000-2019	RWEQ	Central Asia	3.45	3.17	(Wang et al., 2020)
2000-2020	RWEQ	Central Asia	1.98-5.06	3.21	(Yu et al., 2024)
1991-2020	RWEQ	Southern Africa	4.64	4.57	(Zhao et al., 2021)
2001-2020	RWEQ	Africa	16.67	13.27	(Zhang et al., 2024a)

4.2 Advantages of the 8-Day Temporal Resolution

This study refined the event scale of investigation from a monthly to an 8-day scale. This finer temporal resolution enables a more accurate capture of the rapid dynamic changes in key driving factors such as wind speed, precipitation, soil moisture, and vegetation cover. The wind erosion process is primarily driven by instantaneous wind force, with short-duration strong wind events serving as the core dynamic mechanism triggering soil loss. Traditional low-temporal-resolution data (e.g., monthly or annual averages) may smooth out these brief yet high-intensity wind speed peaks, thereby

https://doi.org/10.5194/essd-2026-66
Preprint. Discussion started: 10 February 2026

underestimating the actual intensity and frequency of wind erosion (Shen et al., 2019). Furthermore, mismatches between different variables, such as the misalignment between the vegetation growing season and peak wind speed periods, can also lead to underestimation in low-temporal-resolution assessments (Zhang et al., 2019b). Therefore, compared to low-temporal-resolution data like monthly or annual scales, the 8-day scale can effectively capture such episodic strong wind events that cause significant erosion. This avoids underestimating actual wind erosion amounts due to data smoothing and allows for a more precise calculation of the wind factor and quantification of its contribution to the erosion process.

Secondly, wind erosion is not a continuous and uniform process but rather consists of a series of discrete events of varying intensity and duration (Shen et al., 2018). High temporal resolution is therefore crucial for analyzing the episodic characteristics of wind erosion. Employing an 8-day assessment unit allows for better isolation and quantification of these short-term, high-intensity erosion events, preventing them from being obscured within long-term averages and thus providing a more realistic reflection of the actual risk patterns and spatiotemporal variation of wind erosion. Furthermore, high-resolution data is particularly important for studying extreme wind erosion events. By utilizing long-term 8-day resolution data, it is possible to analyze the frequency and intensity trends of extreme wind erosion events, and their association with climate change, such as increased droughts and strong wind events.

From an application perspective, the 8-day resolution wind erosion assessment results provide a more detailed basis for decision-making in formulating timely and precise prevention and mitigation strategies. It enables decision-makers to identify short-term threat windows for wind erosion in specific areas, thereby optimizing farming management, adjusting the timing of vegetation restoration projects, or enhancing the targeting of dust storm warnings. This holds clear practical value for ecological protection and sustainable land management in wind erosion-active regions such as northern China and Central Asia. In summary, adopting an 8-day temporal resolution in global-scale assessments significantly enhances the depth of understanding of wind erosion dynamic processes, the accuracy of simulation, and the timeliness of management support.

4.3 Limitations and Future Improvements

This study made progress in global wind erosion assessment, but it still has several limitations, primarily stemming from data availability and simplifications in model parameterization. Due to constraints in the availability and consistency of global-scale data, this study assigned specific values to certain parameters, which may introduce uncertainties. For example, the threshold wind speed for erosion onset typically exhibits spatial heterogeneity depending on land use type, surface roughness, and topsoil conditions, but this study uniformly set it to 5 m/s. This simplification may lead to overestimating or underestimating the frequency and intensity of wind erosion under certain surface conditions. Furthermore, due to the lack of detailed global data on crop types and field management practices for cultivated land, the model was unable to differentiate the distinct effects of standing residues versus flat residues on surface cover and aerodynamic roughness. This may result in a systematic overestimation of wind erosion on cropland. Although cropland is not a primary contributor to the global total wind erosion, thus making the impact of this bias on the overall assessment relatively limited, incorporating detailed

https://doi.org/10.5194/essd-2026-66
Preprint. Discussion started: 10 February 2026

agricultural parameters (such as crop types, rotation systems, and residue management) holds significant importance for enhancing assessment accuracy in regional or local-scale refined wind erosion modeling.

5 Data availability

The GloWE-8D dataset is publicly available in GeoTIFF format via Zenodo at https://zenodo.org/records/18245214 (Zhang et al., 2026). It features a spatial resolution of 0.05°, a temporal resolution of 8 days, and covers the period from 1982 to 2020, with data units expressed as t/km². The data for each year are stored in separate compressed files.

6 Conclusions

Based on the RWEQ and integrating multi-source data, including ERA5 reanalysis meteorological data, GLASS fractional vegetation cover, GLC_FCS30D land use data, and SoilGrids soil properties, this study constructed, for the first time, a wind erosion assessment dataset at a global scale spanning 1982–2020 with an 8-day temporal resolution and a 0.05° spatial resolution. By introducing a residue factor scheme based on growing season identification, the representation accuracy of wind erosion suppression during vegetation cover periods was enhanced, achieving continuous, high spatiotemporal resolution monitoring of global wind erosion processes. The spatial distribution of this dataset showed good consistency with MERRA-2 dust emission data (R^2=0.79), and its temporal variations were significantly correlated with coarse-mode aerosol optical depth observations from AERONET stations, validating its reliability in characterizing the spatiotemporal patterns of wind erosion. Comparisons with existing regional studies indicated that the assessment results are within the same order of magnitude and exhibit high spatial correlation with wind erosion intensities in most typical regions, demonstrating the dataset's reasonableness and comparability. As the first publicly available, long-term, high spatiotemporal resolution global wind erosion data product, this dataset enables a more refined capture of the intermittent and episodic characteristics of wind erosion, revealing its seasonal dynamics and long-term trends, thereby providing an important data foundation for global and regional dust emission estimation and the formulation of land degradation prevention strategies.

Author contributions

HZ proposed the ideas, produced the datasets, and performed the data analysis and visualization. HZ prepared the manuscript with contributions from all co-authors. JP supervised the production and revised the manuscript. All authors reviewed and revised the manuscript.

https://doi.org/10.5194/essd-2026-66
Preprint. Discussion started: 10 February 2026

Competing interests

The contact author has declared that none of the authors has any competing interests.

Disclaimer

Publisher's note: Copernicus Publications remains neutral with regard to jurisdictional claims in published maps and institutional affiliations.

Financial support

This research was financially supported by the National Natural Science Foundation of China (42430502)

References

Alewell, C., Ringeval, B., Ballabio, C., Robinson, D. A., Panagos, P., and Borrelli, P.: Global phosphorus shortage will be aggravated by soil erosion, Nat. Commun., 11, 4546, https://doi.org/10.1038/s41467-020-18326-7, 2020.

Bexell, M. and Jönsson, K.: Responsibility and the united nations' sustainable development goals, Forum Dev. Stud., 44, 13–29, https://doi.org/10.1080/08039410.2016.1252424, 2017.

Borrelli, P., Alewell, C., Alvarez, P., Anache, J. A. A., Baartman, J., Ballabio, C., Bezak, N., Biddoccu, M., Cerdà, A., Chalise, D., Chen, S., Chen, W., De Girolamo, A. M., Gessesse, G. D., Deumlich, D., Diodato, N., Efthimiou, N., Erpul, G., Fiener, P., Freppaz, M., Gentile, F., Gericke, A., Haregeweyn, N., Hu, B., Jeanneau, A., Kaffas, K., Kiani-Harchegani, M., Villuendas, I. L., Li, C., Lombardo, L., López-Vicente, M., Lucas-Borja, M. E., Märker, M., Matthews, F., Miao, C., Mikoš, M., Modugno, S., Möller, M., Naipal, V., Nearing, M., Owusu, S., Panday, D., Patault, E., Patriche, C. V., Poggio, L., Portes, R., Quijano, L., Rahdari, M. R., Renima, M., Ricci, G. F., Rodrigo-Comino, J., Saia, S., Samani, A. N., Schillaci, C., Syrris, V., Kim, H. S., Spinola, D. N., Oliveira, P. T., Teng, H., Thapa, R., Vantas, K., Vieira, D., Yang, J. E., Yin, S., Zema, D. A., Zhao, G., and Panagos, P.: Soil erosion modelling: a global review and statistical analysis, Sci. Total Environ., 780, 146494, https://doi.org/10.1016/j.scitotenv.2021.146494, 2021.

Borrelli, P., Panagos, P., Alewell, C., Ballabio, C., de Oliveira Fagundes, H., Haregeweyn, N., Lugato, E., Maerker, M., Poesen, J., Vanmaercke, M., and Robinson, D. A.: Policy implications of multiple concurrent soil erosion processes in european farmland, Nat. Sustainability, 6, 103–112, https://doi.org/10.1038/s41893-022-00988-4, 2023.

Chappell, A., Baldock, J., and Sanderman, J.: The global significance of omitting soil erosion from soil organic carbon cycling schemes, Nature Clim Change, 6, 187–191, https://doi.org/10.1038/nclimate2829, 2016.

Chappell, A., Webb, N. P., Leys, J. F., Waters, C. M., Orgill, S., and Eyres, M. J.: Minimising soil organic carbon erosion by wind is critical for land degradation neutrality, Environ. Sci. Policy, 93, 43–52, https://doi.org/10.1016/j.envsci.2018.12.020, 2019.

Chappell, A., Webb, N. P., Hennen, M., Schepanski, K., Ciais, P., Balkanski, Y., Zender, C. S., Tegen, I., Zeng, Z., Tong, D., Baker, B., Ekström, M., Baddock, M., Eckardt, F. D., Kandakji, T., Lee, J. A., Nobakht, M., von Holdt, J., and Leys, J. F.:

https://doi.org/10.5194/essd-2026-66
Preprint. Discussion started: 10 February 2026

Satellites reveal Earth's seasonally shifting dust emission sources, Science of The Total Environment, 883, 163452, https://doi.org/10.1016/j.scitotenv.2023.163452, 2023.

Chappell, A., Hennen, M., Schepanski, K., Dhital, S., and Tong, D.: Reducing Resolution Dependency of Dust Emission Modeling Using Albedo-Based Wind Friction, Geophysical Research Letters, 51, e2023GL106540, https://doi.org/10.1029/2023GL106540, 2024.

Chi, W., Zhao, Y., Kuang, W., and He, H.: Impacts of anthropogenic land use/cover changes on soil wind erosion in China, Science of The Total Environment, 668, 204–215, https://doi.org/10.1016/j.scitotenv.2019.03.015, 2019.

Chi, W., Wang, Y., Lou, Y., Na, Y., Luo, Q., Chi, W., Wang, Y., Lou, Y., Na, Y., and Luo, Q.: Effect of Land Use/Cover Change on Soil Wind Erosion in the Yellow River Basin since the 1990s, Sustainability, 14, https://doi.org/10.3390/su141912930, 2022.

Chu, Z., Liu, M., Zhang, Q., Cai, X., Zhang, Y., Hu, T., Qiu, X., Huang, Z., and Wang, X.: Spatiotemporal distribution of global wind erosion over the past four decades, Environ. Res. Lett., 19, 114019, https://doi.org/10.1088/1748-9326/ad7d22, 2024.

Dang, X., Na, Y., Chi, W., Zhao, J., Zhao, Y., Wang, Y., Wu, X., and Wang, Y.: Spatio-Temporal Evolution of Sandy Land and its Impact on Soil Wind Erosion in the Kubuqi Desert in Recent 30 Years, Frontiers in Environmental Science, 10, https://doi.org/10.3389/fenvs.2022.950196, 2022.

Duniway, M. C., Pfennigwerth, A. A., Fick, S. E., Nauman, T. W., Belnap, J., and Barger, N. N.: Wind erosion and dust from US drylands: a review of causes, consequences, and solutions in a changing world, Ecosphere, 10, e02650, https://doi.org/10.1002/ecs2.2650, 2019.

Feng, S., Zhao, W., Yan, J., Xia, F., Wang, H., Zhou, A., and Pereira, P.: Vegetation restoration contributes to a reduction in wind and water erosion in China's drylands, Applied Geography, 176, 103517, https://doi.org/10.1016/j.apgeog.2025.103517, 2025.

Fryrear, D. W., Bilbro, J. D., Saleh, A., Schomberg, H., Stout, J. E., and Zobeck, T. M.: RWEQ: Improved wind erosion technology, Journal of Soil and Water Conservation, 55, 183–189, 2000.

Funk, R.: Assessment and measurement of wind erosion, in: Novel methods for monitoring and managing land and water resources in siberia, edited by: Mueller, L., Sheudshen, A. K., and Eulenstein, F., Springer International Publishing, Cham, 425–449, https://doi.org/10.1007/978-3-319-24409-9_18, 2016.

Gao, X., Zhang, H., Huang, L., Fan, J., Liu, X., Cao, W., Liu, H., and Liu, G.: Where, When, and How Much Should We Pay for Wind Erosion Prevention Services of the Largest Chinese Grassland Reserve?, Environ. Sci. Technol., 58, 2615–2626, https://doi.org/10.1021/acs.est.3c03327, 2024.

Ginoux, P., Prospero, J. M., Torres, O., and Chin, M.: Long-term simulation of global dust distribution with the GOCART model: correlation with north atlantic oscillation, Environ. Modell. Software, 19, 113–128, https://doi.org/10.1016/S1364-8152(03)00114-2, 2004.

Gong, G., Liu, J., Shao, Q., and Zhai, J.: Sand-Fixing Function under the Change of Vegetation Coverage in a Wind Erosion Area in Northern China, in: Journal of Resources and Ecology, journalAbbreviation: Journal of Resources and Ecology, 105–114, https://doi.org/10.5814/j.issn.1674-764x.2014.02.002, 2014.

https://doi.org/10.5194/essd-2026-66
Preprint. Discussion started: 10 February 2026

Gu, H., Qiao, Y., Xi, Z., Rossi, S., Smith, N. G., Liu, J., and Chen, L.: Warming-induced increase in carbon uptake is linked to earlier spring phenology in temperate and boreal forests, Nat. Commun., 13, 3698, https://doi.org/10.1038/s41467-022-31496-w, 2022.

Guo, Z., Zobeck, T. M., Stout, J. E., and Zhang, K.: The effect of wind averaging time on wind erosivity estimation, Earth Surf Processes Landf, 37, 797–802, https://doi.org/10.1002/esp.3222, 2012.

Huang, J., Ji, M., Xie, Y., Wang, S., He, Y., and Ran, J.: Global semi-arid climate change over last 60 years, Clim. Dyn., 46, 1131–1150, https://doi.org/10.1007/s00382-015-2636-8, 2016.

Jarrah, M., Mayel, S., Tatarko, J., Funk, R., and Kuka, K.: A review of wind erosion models: Data requirements, processes, and validity, Catena, 187, 104388, https://doi.org/10.1016/j.catena.2019.104388, 2020.

Jiang, L., Xiao, Y., Zheng, H., and Ouyang, Z.: Spatio-temporal variation of wind erosion in Inner Mongolia of China between 2001 and 2010, Chin. Geogr. Sci., 26, 155–164, https://doi.org/10.1007/s11769-016-0797-y, 2016.

Lackóová, L., Kaletová, T., Halászová, K., Lackóová, L., Kaletová, T., and Halászová, K.: Are drought and wind force driving factors of wind erosion climatic erosivity in a changing climate? A case study in a landlocked country in central europe, Land, 12, https://doi.org/10.3390/land12040757, 2023.

Lal, R.: Soil erosion and the global carbon budget, Environ. Int., 29, 437–450, https://doi.org/10.1016/S0160-4120(02)00192-7, 2003.

Li, C., Fu, B., Wang, S., Stringer, L. C., Wang, Y., Li, Z., Liu, Y., and Zhou, W.: Drivers and impacts of changes in China's drylands, Nat Rev Earth Environ, 2, 858–873, https://doi.org/10.1038/s43017-021-00226-z, 2021.

Li, J., Ma, X., and Zhang, C.: Predicting the spatiotemporal variation in soil wind erosion across Central Asia in response to climate change in the 21st century, Science of The Total Environment, 709, 136060, https://doi.org/10.1016/j.scitotenv.2019.136060, 2020.

Lin, J., Guan, Q., Pan, N., Zhao, R., Yang, L., and Xu, C.: Spatiotemporal variations and driving factors of the potential wind erosion rate in the Hexi region, PR China, Land Degradation & Development, 32, 139–157, https://doi.org/10.1002/ldr.3702, 2021.

Liu, J., Wang, X., Zhang, L., Guo, Z., Chang, C., Du, H., Wang, H., Wang, R., Li, J., Li, Q., Liu, J., Wang, X., Zhang, L., Guo, Z., Chang, C., Du, H., Wang, H., Wang, R., Li, J., and Li, Q.: Regional Potential Wind Erosion Simulation Using Different Models in the Agro-Pastoral Ecotone of Northern China, International Journal of Environmental Research and Public Health, 19, https://doi.org/10.3390/ijerph19159538, 2022a.

Liu, X., Li, L., Qin, F., Li, Y., Chen, J., and Fang, X.: Ecological policies enhanced ecosystem services in the Hunshandak sandy land of China, Ecological Indicators, 144, 109450, https://doi.org/10.1016/j.ecolind.2022.109450, 2022b.

Liu, X., Du, H., Li, S., Liu, X., Fan, Y., and Wang, T.: Dynamics of soil wind erosion in the Mu Us sandy land (in northern China) affected by cropland reclamation from 2000 to 2020, Ecological Indicators, 154, 110717, https://doi.org/10.1016/j.ecolind.2023.110717, 2023.

Ma, X., He, H., Huo, T., Su, Y., and Yan, W.: Reassessing Soil Wind Erosion in Arid Regions of Central Asia: Fully Considering the Contribution of Non-Photosynthetic Vegetation (NPV), Land Degradation & Development, 36, 2489–2503, https://doi.org/10.1002/ldr.5512, 2025.

https://doi.org/10.5194/essd-2026-66
Preprint. Discussion started: 10 February 2026

Mandakh, N., Tsogtbaatar, J., Dash, D., and Khudulmur, S.: Spatial assessment of soil wind erosion using WEQ approach in Mongolia, J. Geogr. Sci., 26, 473–483, https://doi.org/10.1007/s11442-016-1280-5, 2016.

Mei, Y., Batunacun, Hai, C., Chang, A., Chang, Y., Wang, Y., Hu, Y., Mei, Y., Batunacun, Hai, C., Chang, A., Chang, Y., Wang, Y., and Hu, Y.: Spatiotemporal Dynamics and Driving Factors of Soil Wind Erosion in Inner Mongolia, China, Remote Sensing, 17, https://doi.org/10.3390/rs17142365, 2025.

Sharratt, B. S., Tatarko, J., Abatzoglou, J. T., Fox, F. A., and Huggins, D.: Implications of climate change on wind erosion of agricultural lands in the Columbia plateau, Weather and Climate Extremes, 10, 20–31, https://doi.org/10.1016/j.wace.2015.06.001, 2015.

Shen, Y., Zhang, C., Wang, X., Zou, X., and Kang, L.: Statistical characteristics of wind erosion events in the erosion area of northern China, Catena, 167, 399–410, https://doi.org/10.1016/j.catena.2018.05.020, 2018.

Shen, Y., Zhang, C., Huang, X., Wang, X., and Cen, S.: The effect of wind speed averaging time on sand transport estimates, Catena, 175, 286–293, https://doi.org/10.1016/j.catena.2018.12.020, 2019.

Shi, S., Yang, P., Vrieling, A., and Tol, C. van der: Vegetation optimal temperature modulates global vegetation season onset shifts in response to warming climate, Commun Earth Environ, 6, 203, https://doi.org/10.1038/s43247-025-02186-4, 2025.

Sun, R., He, H., Jing, Y., Leng, S., Yang, G., Lü, Y., Borrelli, P., Chen, L., and Fu, B.: Global Wind Erosion Reduction Driven by Changing Climate and Land Use, Earth's Future, 12, e2024EF004930, https://doi.org/10.1029/2024EF004930, 2024.

Tanaka, T. Y. and Chiba, M.: A numerical study of the contributions of dust source regions to the global dust budget, Global Planet. Change, 52, 88–104, https://doi.org/10.1016/j.gloplacha.2006.02.002, 2006.

Tao, W., Liu, S., Wang, Q., Su, L., and Sun, Y.: Spatiotemporal Characteristics of Soil Erosion on the Chinese Loess Plateau and Strategies for Vegetation Management, J Soil Sci Plant Nutr, 24, 4439–4456, https://doi.org/10.1007/s42729-024-01846-2, 2024.

Tuo, D., Xu, M., and Gao, G.: Relative contributions of wind and water erosion to total soil loss and its effect on soil properties in sloping croplands of the Chinese Loess Plateau, Sci. Total Environ., 633, 1032–1040, https://doi.org/10.1016/j.scitotenv.2018.03.237, 2018.

Van Pelt, R. S., Zobeck, T. M., Potter, K. N., Stout, J. E., and Popham, T. W.: Validation of the wind erosion stochastic simulator (WESS) and the revised wind erosion equation (RWEQ) for single events, Environ. Modell. Software, 19, 191–198, https://doi.org/10.1016/S1364-8152(03)00122-1, 2004.

Wang, S., Xu, X., Huang, L., Wang, S., Xu, X., and Huang, L.: Spatial and Temporal Variability of Soil Erosion in Northeast China from 2000 to 2020, Remote Sensing, 15, https://doi.org/10.3390/rs15010225, 2022.

Wang, S., Xu, X., Wang, S., and Xu, X.: Spatiotemporal Variation in Soil Wind Erosion in the Northern Slope of the Tianshan Mountains from 2000 to 2018, Land, 13, https://doi.org/10.3390/land13101604, 2024.

Wang, W., Samat, A., Ge, Y., Ma, L., Tuheti, A., Zou, S., and Abuduwaili, J.: Quantitative Soil Wind Erosion Potential Mapping for Central Asia Using the Google Earth Engine Platform, Remote Sensing, 12, 3430, https://doi.org/10.3390/rs12203430, 2020.

Wei, X., Wu, X., Wang, D., Wu, T., Li, R., Hu, G., Zou, D., Bai, K., Ma, X., Liu, Y., Yan, X., Fan, X., Cao, X., and Dashtseren, A.: Spatiotemporal variations and driving factors for potential wind erosion on the Mongolian Plateau, Science of The Total Environment, 862, 160829, https://doi.org/10.1016/j.scitotenv.2022.160829, 2023.

Wu, J., Zheng, X., Zhao, L., Fan, J., Liu, J., Wu, J., Zheng, X., Zhao, L., Fan, J., and Liu, J.: Effects of Ecological Programs and Other Factors on Soil Wind Erosion between 1981–2020, Remote Sensing, 14, https://doi.org/10.3390/rs14215322, 2022.

Yang, G., Sun, R., Jing, Y., Xiong, M., Li, J., and Chen, L.: Global assessment of wind erosion based on a spatially distributed RWEQ model, Progress in Physical Geography: Earth and Environment, 030913332110306, https://doi.org/10.1177/03091333211030608, 2021.

Yu, W., Ma, X., Yan, W., Wang, Y., Yu, W., Ma, X., Yan, W., and Wang, Y.: Assessment of Soil Wind Erosion and Population Exposure Risk in Central Asia's Terminal Lake Basins, Water, 16, https://doi.org/10.3390/w16131911, 2024.

Yue, Y., Shi, P., Zou, X., Ye, X., Zhu, A., and Wang, J.: The measurement of wind erosion through field survey and remote sensing: a case study of the Mu Us Desert, China, Nat Hazards, 76, 1497–1514, https://doi.org/10.1007/s11069-014-1516-6, 2015.

Zhang, G., Azorin-Molina, C., Shi, P., Lin, D., Guijarro, J. A., Kong, F., and Chen, D.: Impact of near-surface wind speed variability on wind erosion in the eastern agro-pastoral transitional zone of Northern China, 1982–2016, Agricultural and Forest Meteorology, 271, 102–115, https://doi.org/10.1016/j.agrformet.2019.02.039, 2019a.

Zhang, H., Fan, J., Cao, W., Harris, W., Li, Y., Chi, W., and Wang, S.: Response of wind erosion dynamics to climate change and human activity in Inner Mongolia, China during 1990 to 2015, Science of The Total Environment, 639, 1038–1050, https://doi.org/10.1016/j.scitotenv.2018.05.082, 2018.

Zhang, H., Gao, Y., Sun, D., Liu, L., Cui, Y., and Zhu, W.: Wind Erosion Changes in a Semi-Arid Sandy Area, Inner Mongolia, China, Sustainability, 11, 188, https://doi.org/10.3390/su11010188, 2019b.

Zhang, H., Peng, J., Zhao, C., Xu, Z., Dong, J., and Gao, Y.: Wind speed in spring dominated the decrease in wind erosion across the Horqin Sandy Land in northern China, Ecological Indicators, 127, 107599, https://doi.org/10.1016/j.ecolind.2021.107599, 2021.

Zhang, H., Peng, J., and Zhao, C.: Wind Speed and Vegetation Coverage in Turn Dominated Wind Erosion Change With Increasing Aridity in Africa, Earth's Future, 12, e2024EF004468, https://doi.org/10.1029/2024EF004468, 2024a.

Zhang, L., Guo, Z., Li, J., Chang, C., Wang, R., and Li, Q.: Effect of the Type of Wind Data on Regional Potential Wind Erosion Estimation, Front. Environ. Sci., 10, https://doi.org/10.3389/fenvs.2022.847128, 2022a.

Zhang, T., Li, D., East, A. E., Walling, D. E., Lane, S., Overeem, I., Beylich, A. A., Koppes, M., and Lu, X.: Warming-driven erosion and sediment transport in cold regions, Nat. Rev. Earth Environ., 3, 832–851, https://doi.org/10.1038/s43017-022-00362-0, 2022b.

Zhang, X., Zhang, C., Zuo, X., Zou, X., Wang, X., Zhao, J., Li, W., Zhou, Z., and Zhang, Y.: Extension of the revised wind erosion equation (RWEQ) to calculate grassland wind erosion rates based on the 137Cs tracing technique, CATENA, 234, 107544, https://doi.org/10.1016/j.catena.2023.107544, 2024b.

Zhang, X., Zhao, T., Xu, H., Liu, W., Wang, J., Chen, X., and Liu, L.: GLC_FCS30D: the first global 30 m land-cover dynamics monitoring product with a fine classification system for the period from 1985 to 2022 generated using

https://doi.org/10.5194/essd-2026-66
Preprint. Discussion started: 10 February 2026

620 dense-time-series landsat imagery and the continuous change-detection method, Earth Syst. Sci. Data, 16, 1353–1381, https://doi.org/10.5194/essd-16-1353-2024, 2024c.

Zhao, C., Zhang, H., Wang, M., Jiang, H., Peng, J., and Wang, Y.: Impacts of climate change on wind erosion in Southern Africa between 1991 and 2015, Land Degradation & Development, 32, 2169–2182, https://doi.org/10.1002/ldr.3895, 2021.

Zhou, A., Zhao, W., Han, Y., Zhang, S., and Pereira, P.: Effects and benefits of wind erosion prevention in China's dryland
625 and surrounding countries, Catena, 251, 108812, https://doi.org/10.1016/j.catena.2025.108812, 2025.